Intercomparison of dissolved iron isotope profiles from reoccupation of three GEOTRACES stations in the Atlantic Ocean

T.M. Conway [a,b,*], S.G. John [b,1], F. Lacan [c]

[a] Department of Earth Sciences, ETH Zürich, Zürich, Switzerland
[b] Department of Earth and Ocean Sciences, University of South Carolina, Columbia, SC, United States
[c] LEGOS, Université de Toulouse, CNES, CNRS, IRD, UPS, Toulouse, France

ARTICLE INFO

ABSTRACT

Intercomparison of trace metal data is a key aspect of the International GEOTRACES program, allowing data from multiple laboratories and countries to be combined to produce high-resolution datasets for the oceans. The use of crossover stations by the GEOTRACES program provides the opportunity both for comparison of analytical techniques and assessment of temporal variability in the cycling of trace metals such as iron (Fe). Here, we present the first comparison of dissolved Fe stable isotope ratio (δ^{56}Fe; relative to IRMM-014) profiles in the oceans, from reoccupations of three locations in the Atlantic Ocean; (1) the Bermuda Atlantic Time Series station (31.75°N 64.17°W) during the US GEOTRACES IC1 cruise (June 2008) and the US GEOTRACES GA03 cruise (Nov. 2011); (2) the Tenatso Time Series station near Cape Verde (17.4°N 24.5°W) during the U.S GEOTRACES GA03 cruises (2010; 2011), and (3) a station in the Cape Basin close to South West Africa (31.1–31.4°S 36.5°W) during the French GEOTRACES GIPY4 Bonus Good Hope Cruise (Feb. 2008) and the UK GEOTRACES GA10 D357 cruise (Oct. 2010). These datasets provided us with the opportunity not only to compare sampling and analysis techniques by two different laboratories (USC and LEGOS), but also the temporal variability of δ^{56}Fe at these locations on a 1–3 year timescale. We found that a good agreement between data and profiles generated by different laboratories does allow assessment of temporal variation of δ^{56}Fe in the water column, as well as spatial variability and synthesis of datasets from different regions of the ocean. In fact, comparison of δ^{56}Fe at the three locations in this study demonstrates a remarkable consistency between the shapes of ocean δ^{56}Fe profiles measured 1–3 years apart, pointing to the overall stability of Fe cycling at all three locations on these timescales, despite the expected dynamic nature of the Fe cycle. This consistency is highlighted by strong agreement in δ^{56}Fe throughout the whole water-column at Bermuda, and in waters deeper than 500 m in the Cape Basin, which suggests that different water masses may carry distinct δ^{56}Fe signatures. In contrast to these stable δ^{56}Fe, we did observe apparent temporal variability in δ^{56}Fe between cruises at other locations and in surface waters, both throughout the water column at Cape Verde, and in Agulhas-leakage influenced surface waters in the Cape Basin. Such temporal variability may thus provide information about changes in internal Fe cycling or external Fe sources on these timescales. Overall, this study highlights the usefulness of repeat δ^{56}Fe measurements to provide information on the variability of Fe cycling throughout the oceans.

© 2016 Elsevier B.V. All rights reserved.

1. Introduction

Seawater dissolved iron (Fe) is an important limiting nutrient for phytoplankton over much of the surface oceans (Moore et al., 2001). Understanding the global distribution and biogeochemical cycling of Fe is a central aim of the international GEOTRACES program which seeks to measure global distributions of a range of trace elements and their isotopes. Fe concentrations are a GEOTRACES key parameter, meaning their analysis is required on all GEOTRACES cruises (Anderson and Henderson, 2005; Henderson et al., 2007). Fe stable isotopes (δ^{56}Fe) have also been measured on several GEOTRACES cruises, although they are not a key parameter. The resulting ocean sections of dissolved Fe concentration from the Atlantic, Indian and Pacific Oceans, and similar sections in progress, are beginning to provide new insights into the marine sources, sinks and cycling of Fe at both the regional and global scale throughout the oceans (e.g. Conway and John, 2014a; Klunder et al., 2012; Nishioka et al., 2013; Resing et al., 2015; Rijkenberg et al., 2014; Saito et al., 2013).

GEOTRACES cruises all follow internationally agreed methods for clean sampling and handling (The GEOTRACES Cookbook; Cutter et al.,

---

* Corresponding author at: Department of Earth Sciences, ETH Zürich, Zürich, Switzerland.
E-mail address: conway.tm@gmail.com (T.M. Conway).
[1] Department of Earth Sciences, University of Southern California, Los Angeles, USA (present address).

2010, 2014), meaning that datasets can be collated to form regional and global pictures of the distribution of trace metals and their isotopes in the ocean. Recently, such data has been combined to form the GEOTRACES Intermediate Data Product and the GEOTRACES eAtlas (Mawji et al., 2015; Schlitzer, 2015). To ensure compatibility of datasets from different groups and nations, given the range of collection and analytical techniques deployed on different cruises, it is essential to carry out intercomparison of data collected from the same location and/or in the same samples by multiple groups. Accordingly, intercomparison is an important aspect of the GEOTRACES program, with the recommended reporting of measurements of SAFe reference standards for dissolved trace metal concentrations, the use of cross-over stations for comparison between different GEOTRACES cruises (see Fig. 1), and a number of studies comparing sampling systems (Cutter, 2013). Intercomparison of trace metal concentrations and stable isotope ratios was a goal of two US GEOTRACES cruises in the Atlantic (IC1, June 2008) and North Pacific (IC2, May 2009) Oceans (Boyle et al., 2012; Cutter and Bruland, 2012; Cutter, 2013; and others), and recent work has compared the clean sampling system of the Dutch and US GEOTRACES programs as well as different analytical techniques (Middag et al., 2015).

The GEOTRACES program and similar cruises have also facilitated the application of dissolved Fe isotope ratios (δ^{56}Fe) as a useful parameter for understanding the marine Fe cycle. Although a challenging measurement, due to the low concentration of Fe in seawater and the difficulties of analysis, advancement in chemical techniques and high-resolution mass spectrometry has allowed a number of groups to develop methods to measure seawater-dissolved δ^{56}Fe over the full range of observed oceanic dissolved Fe concentrations (~0.02 to >2 nmol kg^{-1}). These methods have utilized either NTA or Nobias PA-1 chelating resins (Boyle et al., 2012; Conway et al., 2013a; John and Adkins, 2010; Lacan et al., 2010, 2008; Rouxel and Auro, 2010), extraction with dithiocarbamate (Ellwood et al., 2014) or co-precipitation with magnesium (de

Jong et al., 2007), followed by analysis with multicollector Inductively Coupled Plasma Mass Spectrometry (MC-ICPMS). Such methods have to date led to the publication of dissolved δ^{56}Fe depth profiles from a number of ocean basins (e.g. Chever et al., 2015; John and Adkins, 2012; John et al., 2012; Labatut et al., 2014; Lacan et al., 2008; Radic et al., 2011; Staubwasser et al., 2013), and a high resolution ocean section of dissolved δ^{56}Fe across the North Atlantic (Conway and John, 2014a). Dissolved δ^{56}Fe measurements were also part of the focus of a previous intercomparison effort utilizing seawater collected from the Bermuda Atlantic Time Series onboard the US GEOTRACES 1C1 cruise in 2008, where four different laboratories demonstrated strong agreement on both surface and deep water samples at concentrations of 0.4 and 0.8 nmol kg^{-1} (Boyle et al., 2012; see Fig. 2c–d).

Different marine sources of Fe have different δ^{56}Fe signatures, and these isotope signatures have been used to trace Fe as it mixes through the oceanic water column, including non-reductive sediment dissolution (Labatut et al., 2014; Radic et al., 2011), reductive sediment dissolution (Chever et al., 2015; John et al., 2012), and Fe from multiple sources (Conway and John, 2014a). As such, studies of seawater-dissolved δ^{56}Fe show promise for understanding the cycling and differing sources of Fe to the ocean; however, application of this tracer is still limited to a small number of laboratories. Thus, spatial coverage of δ^{56}Fe measurements throughout the oceans remains sparse. Additionally, although changing conditions over time are important to our understanding of changes in Fe sources and cycling, logistics and cost have meant that repeat-sampling to assess temporal variability has rarely been carried out. However, reoccupation of crossover stations as part of the GEOTRACES program provides us with the opportunity to begin to address this lack of knowledge of variability, as well as to compare sampling and analysis by different groups.

Here we compare measured Fe and δ^{56}Fe profiles from three locations in the Atlantic Ocean (Fig. 1): 1) reoccupation of a GEOTRACES
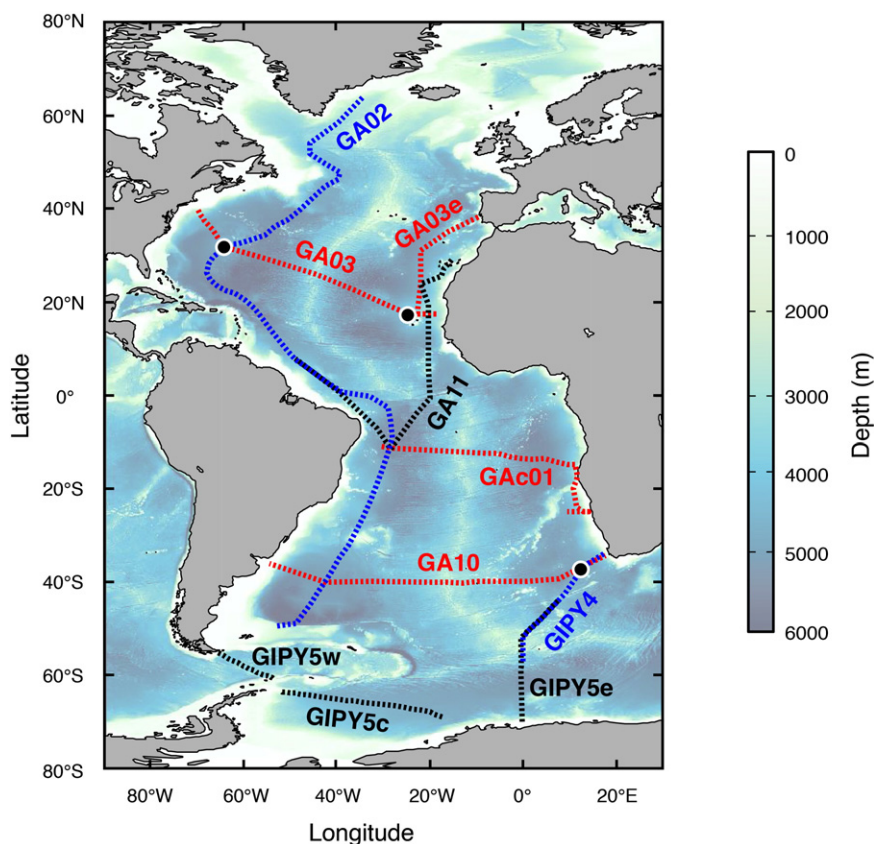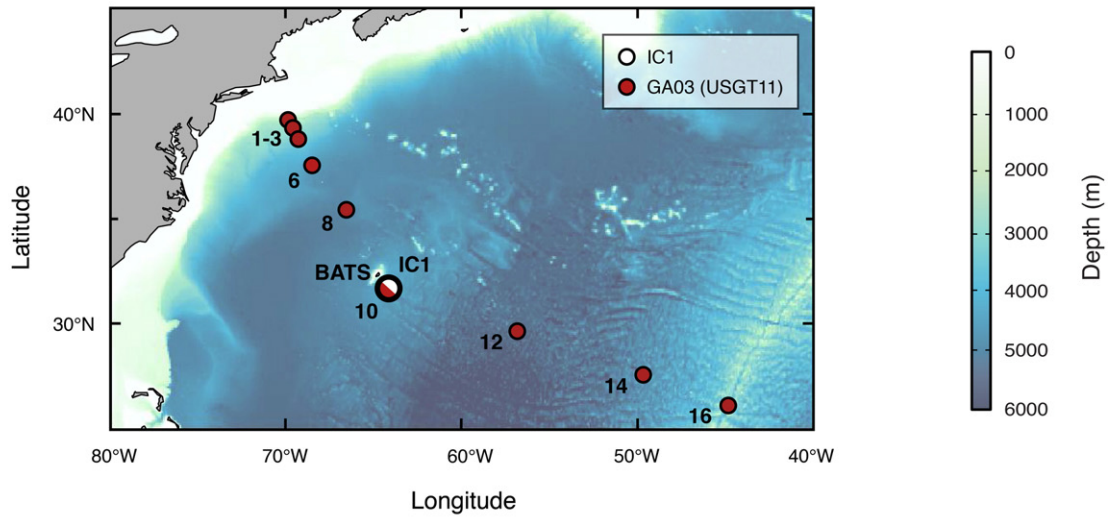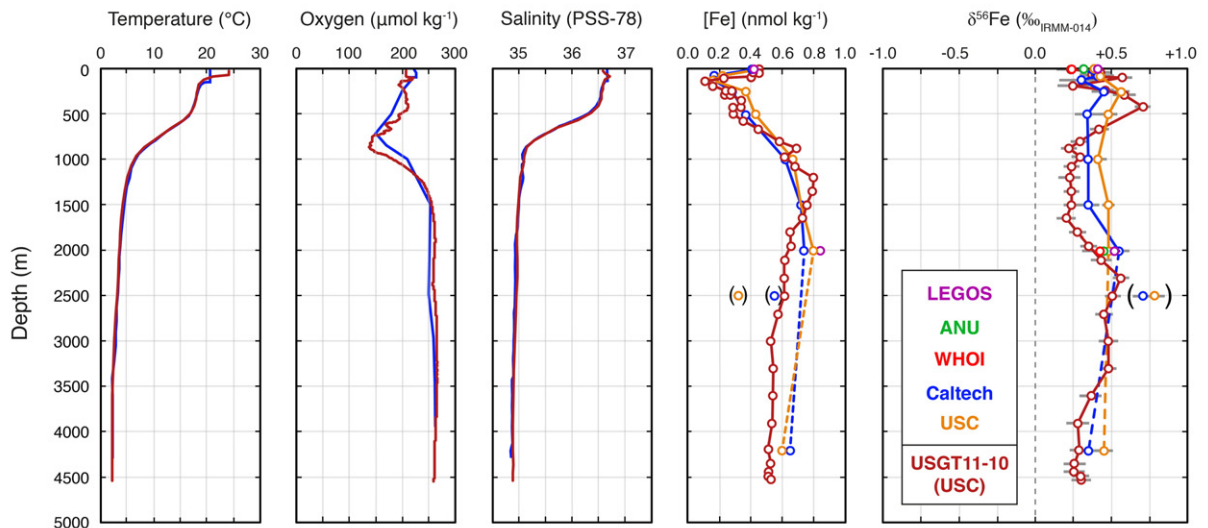

Fig. 1. Atlantic Ocean showing GEOTRACES crossover stations and locations described in this study. Cruises that included in the GEOTRACES Intermediate data product 2014 are shown for reference, based on eGEOTRACES graphics (Mawji et al., 2015; Schlitzer, 2015). The three locations sampled in this study are shown as black dots.
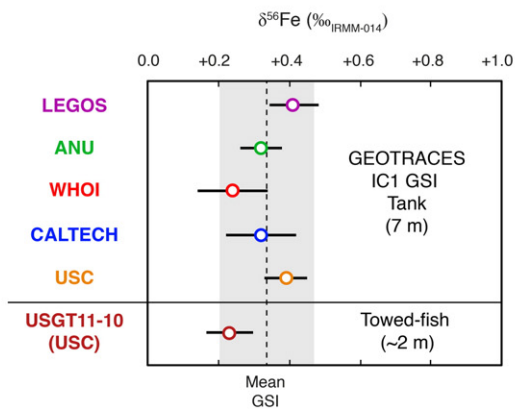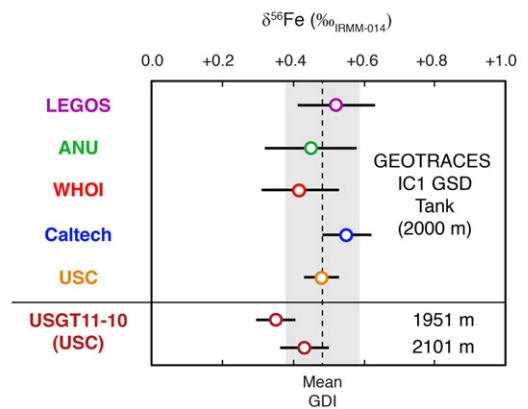
a) Location Map

b) BATS Water column

c) Surface (<10 m)

d) Deep (1950-2100 m)

crossover station at the Bermuda Atlantic Time Series (BATS; 31.75°N 64.17°W; Fig. 2a) by the US GEOTRACES 1C1 cruise in June 2008 and the US GEOTRACES GA03 KN204 cruise in Nov. 2011 (Superstation USGT11–10) allows us to compare δ^{56}Fe data measured by Conway and John (USC; GA03; Conway and John, 2014a) with δ^{56}Fe data measured by five laboratories on the IC1 cruise (Boyle et al., 2012). 2) reoccupation of the Tenatso Time Series station near Cape Verde (17.4°N 24.5°W) by the 2010 (KN204) and 2011 (KN199) cruises of the US GEOTRACES GA03 section (USGT10–12 in Nov. 2010, USGT11–24 in Dec. 2011; Fig. 3a) allows us to compare δ^{56}Fe profiles at this location a year apart. 3) reoccupation of a GEOTRACES crossover station in the South Atlantic by the UK GEOTRACES GA10 D357 Cruise in 2010 (Superstation 3; 31.4°S 36.5°W) and the French GEOTRACES GIPY4 Bonus Good Hope Cruise in 2008 (Superstation S1; 31.1°S 36.5°W) allows us to compare δ^{56}Fe profiles from nearby locations three years apart (Fig. 4a), measured using different collection and analytical techniques by Conway and John (GA10; USC) and Lacan (GIPY4; LEGOS). Interpretation of the δ^{56}Fe profiles measured at these locations is the focus of other articles (Abadie et al., in review; Conway and John, 2014a; John and Adkins, 2012), and so here we instead focus largely on intercomparison and assessment of temporal variability of Fe and δ^{56}Fe.

2. Materials and methods

2.1. Seawater collection and handling

2.1.1. US GEOTRACES IC1 cruise and GA03 section cruises

Seawater collection and sampling were previously described for these cruises by Boyle et al. (2012) and Conway and John (2014a), but are briefly summarized here for ease of reference. Clean seawater was collected similarly on all three US GEOTRACES cruises (IC1, KN199, KN204) onboard the RV Knorr, using either underway Teflon towed-fish (surface samples; ~2 m; Cutter and Bruland, 2012) or the US GEOTRACES rosette with 24 × 12 L GO-Flo bottles on a Kevlar cable (Cutter and Bruland, 2012). Following collection, the GO-Flo bottles were transferred to a clean van and the water filtered through 0.45 μm Osmonics cartridge filters (towed-fish samples) or 0.2 μm Pall Acropak capsule filters (GO-Flo samples).

As part of IC1 at the BATS station (31.75°N 64.17°W; Figs 1-2) on June 22nd, 2008, a 500 L surface isotope sample (GSI) was pumped from the towed-fish and filtered into a clean 500 L acid-cleaned polyethylene tank, where it was acidified with the equivalent of 1 mL 12 M HCl per liter (Boyle et al., 2012; John and Adkins, 2012). Similarly a 250 L deep isotope sample (GDI) was collected from 2000 m using the GEOTRACES rosette, filtered and then homogenized and acidified in an identical polyethylene tank (Boyle et al., 2012). An 8 point profile for isotope comparison (GPri) from depths of 75–3500 m and a single sample for Fe isotope measurement at 4200 m were also collected using the GEOTRACES rosette and similarly filtered and acidified (Boyle et al., 2012; John and Adkins, 2012). Supporting oceanographic parameters were made shipboard and are taken from John and Adkins (2012).

As part of the GA03 section cruises, seawater samples were collected using towed-fish or GEOTRACES Rosette and water filtered into 1 L acid-cleaned Nalgene low density polyethylene (LDPE) bottles from: 1) Station USGT10–12 (17.40°N 24.50°W; 25 point profile, 2–3498 m) on the 02/11/2010; 2) Superstation USGT11–12 at the BATS station (31.75°N, 37 point profile 2–4526 m) on November 19th–21st, 2011; and 3) Station USGT11–24 (17.40°N 24.50°W; 25 point profile, 2–3517 m) on

December 9th–10th, 2011. (Figs 1–3). Seawater samples were acidified back on shore to pH ~2 with conc. Aristar Ultra HCl. Supporting oceanographic parameters were made shipboard and are supplied by the Ocean Data Facility (Jenkins et al., 2015).

2.1.2. U.K. GEOTRACES GA10 section (D357 cruise)

Seawater samples were collected from Station 3 (13.39°S 36.46°W; 13 point profile, 2–4724 m) on October 23rd, 2010 as part of the GA10 D357 cruise on board the RRS Discovery. Clean seawater samples were collected broadly as described by Wyatt et al. (2014); briefly, seawater was collected into twenty-four 10 L clean Teflon-coated OTE samplers on a Titanium CTD frame on a plasma (polyethylene) rope. The OTE bottles were transferred to a clean container, and water samples were filtered using Millipore 25 mm 0.4 μm polyethersulfone (PES) filters (>75 m depth) or 0.2 μm AcroPak Supor Pall PES capsules (< 75 m depth or fish samples). Filtered seawater was collected into acid-cleaned and seawater-rinsed 1 L Nalgene LDPE bottles. Seawater samples were acidified back on shore to pH ~2 with conc. Aristar Ultra HCl. Salinity, temperature and oxygen were measured shipboard using standard methods as described by Wyatt et al. (2014).

2.1.3. French GIPY4 section

Seawater samples were collected from Super-Station 1 (St. 18) (13.12°S 36.51°W; 9 point profile, 31–4068 m) on February 20th, 2008 as part of the GIPY4 MD166 Bonus Good Hope cruise on board the RV Marion Dufresne. Clean seawater samples were collected and filtered as described previously (Abadie et al. in review; Lacan et al., 2008; Lacan et al., 2010); briefly, 10 L seawater samples were collected into acid-cleaned 12 L Go-Flo bottles mounted on a Kevlar wire. Go-Flo bottles were brought inside a clean container and seawater was filtered using Savillex PFA Teflon filtration units with 0.45 μm 90 mm nucleopore membranes into 10 L flexible LDPE containers with PP closure, within a few hours of collection. Samples were acidified onboard with 1.7 mL per L of 9 M twice-distilled HCl.

2.2. Analytical methods

Stable Fe isotope ratios (δ^{56}Fe) are expressed for all laboratories in this paper in standard delta notation, relative to IRMM-014:

$$\delta^{56}Fe\ (\text{\textperthousand}) = \left[\frac{\frac{^{56}Fe}{^{54}Fe}_{sample}}{\frac{^{56}Fe}{^{54}Fe}_{IRMM-014}} - 1 \right] * 1000$$

#### 2.2.1. IC1 intercomparison exercise

Analytical methods for the four laboratories taking part in the IC-1 exercises were described in full by Boyle et al. (2012) and by the respective labs (John and Adkins, 2012; Lacan et al., 2010, 2008; Rouxel and Auro, 2010), with subsequent analysis by USC described below. For reference, three laboratories (WHOI, Caltech, LEGOS) used extraction of Fe from seawater with Qiagen NTA-Superflow resin, whilst one laboratory used extraction using purified ammonium pyrrolidinedithiocarbamate and sodium diethyldithiocarbamate and chloroform (ANU). All laboratories performed analysis by Thermo Neptune MC-ICPMS, either with Ni and standard-sample bracketing (WHOI, Caltech, ANU) or [57]Fe-[58]Fe double spike technique (LEGOS) for instrumental mass-bias correction.

Fig. 2. Comparison of δ^{56}Fe and Fe data from Bermuda Atlantic Time Series (BATS) in the subtropical North West Atlantic (31.75°N 64.17°W) from the US GEOTRACES IC1 (June 2008) and GA03 cruises (Nov. 2011). a) Regional location map showing BATS and GA03 stations sampled for Fe isotope ratios. b) Dissolved Fe concentration (nmol kg^{-1}) and dissolved δ^{56}Fe (relative to IRRM-014) profiles shown with other oceanographic parameters. c) Dissolved δ^{56}Fe from the IC1 surface tank and from GA03 towed-fish sample. d) Dissolved δ^{56}Fe from the IC1 2000 m depth deep tank and from GA03 rosette samples from similar depths. The dashed lines and gray shaded region in b) and c) represent the mean and 2SD δ^{56}Fe respectively of the five labs that have published measurements for the GSI and GDI tanks. Data are reproduced from Boyle et al. (2012); Conway and John (2014a); Conway et al. (2013a,b); John and Adkins (2012). Error bars for ANU and WHOI are from Boyle et al. (2012), error bars for LEGOS represent 2SD on δ^{56}Fe (see Suppl. data), error bars for Caltech are from John and Adkins (2012) and error bars for USC are from Conway et al. (2013a, 2013b) and Conway and John (2014a). For GA03, temperature and salinity are from the GEOTRACES rosette and dissolved oxygen is from the ODF rosette.
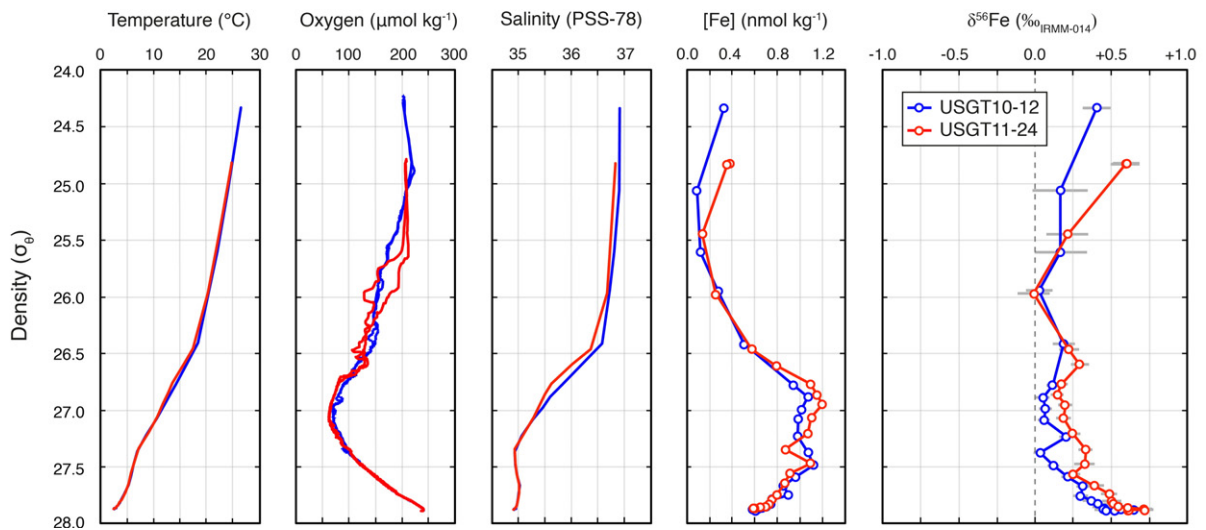
a) Location Map
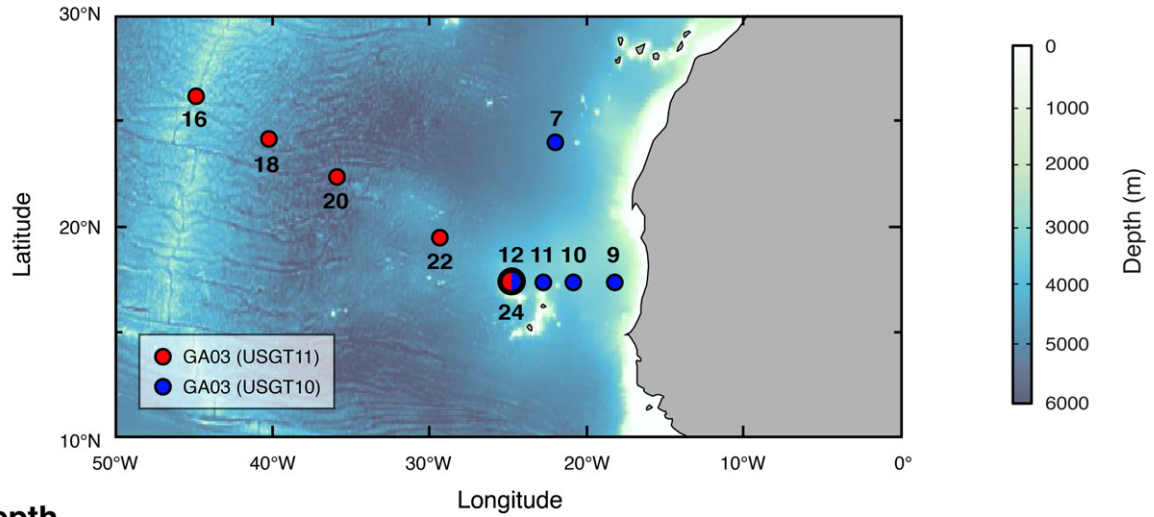
b) vs. Depth
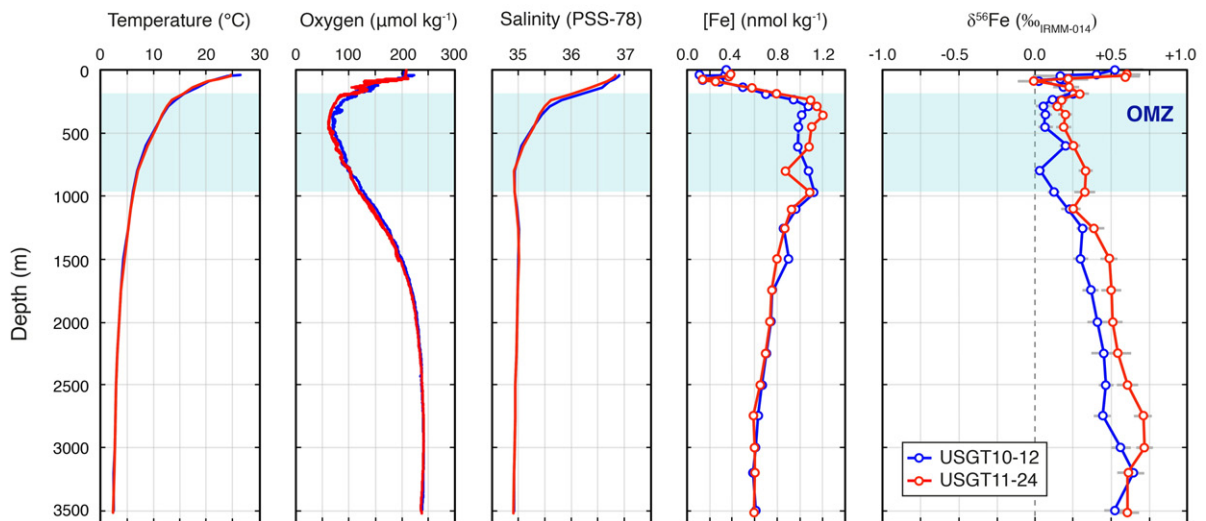
c) vs. Density

Uncertainty on δ^{56}Fe is expressed as 2SE error for ANU and WHOI (Boyle et al., 2012), as 2σ external error for Caltech (John and Adkins., 2012) and as the 2SD on mean δ^{56}Fe for LEGOS (see Suppl. data).

2.2.2. IC1, GA03 and GA10 (USC)

Samples were processed and analyzed at USC for Fe concentration and δ^{56}Fe analysis following several months of storage at pH 2, following already published methods, with extraction by Nobias PA-1, purification by AGMP-1 resin and analysis by Thermo Neptune MC-ICPMS with mass bias correction by ^{57}Fe-^{58}Fe double spike technique (Conway et al., 2013a; Conway and John, 2014a) in 'high' resolution (HR) mode to resolve polyatomic interferences such as ArN$^+$ and ArO$^+$. ^{54}Cr and ^{58}Ni isobaric interferences on ^{54}Fe and ^{58}Fe were corrected for using the measured abundances of ^{53}Cr and ^{60}Ni. A background correction was applied to each sample using the blank 0.1 M HNO$_3$ acid, with this blank acid measured twice for every group of 4–6 samples. δ^{56}Fe were calculated relative to an IRMM-double spike mixture, which was concentration and matrix matched to the samples, and run twice with each group of 4–6 samples. Seawater samples were spiked in a 1:2 sample:spike ratio, purified from 1 L and measured twice by MC-ICPMS with a mean value calculated.

Following Conway et al. (2013a), uncertainty on mean δ^{56}Fe in figures and Suppl. data is expressed as 2σ internal error, calculated from replicates and bracketing standards, based on the previous observation that uncertainty with this technique is dominated by internal error (John, 2012). For this study, 2σ internal analytical error varied from 0.04 to 0.18‰, largely dependent on sample Fe concentration. As an indication of external precision for the method we also calculated the 2SD (0.05‰) of the offset of duplicate analyses from the mean of 60 South Atlantic GA10 seawater samples (0.1–1.8 nmol kg^{-1}), with duplicates measured in different analytical sessions (following Steele et al., 2011). This calculated external precision is similar to or smaller than internal error for most samples, suggesting that for these samples internal error is a good representation of overall uncertainty.

Fe concentration measurements were made via isotope-dilution, with a procedural blank of 0.005 nmol kg^{-1}, with 2% uncertainty applied for weighing and pipetting errors (Conway et al., 2013a). We have previously shown strong agreement with other laboratories for SAFE standards and profile concentration data produced with this method (Conway et al., 2013a; Middag et al., 2015). For some IC1 samples multiple subsamples were purified separately and then each measured twice by MC-ICPMS, with a mean δ^{56}Fe used in figures.

2.2.3. GIPY4 (LEGOS)

Samples were processed and analyzed at LEGOS for δ^{56}Fe following previously described methods (Lacan et al., 2008, 2010). Briefly, Fe was pre-concentrated from 4 to 10 L of seawater using an NTA resin column and then purified with AG 1-×4 anionic exchange resin, before redissolution in ~0.7 mL 0.3 M HNO$_3$ for analysis by MC-ICPMS using a Neptune (Thermo Scientific) coupled with a CETAC Aridus II desolvation system. Instrumental mass bias and potential procedural fractionation was corrected for using the double-spike technique, also following the iterative method of Siebert et al. (2001). A ^{57}Fe-^{58}Fe double spike with a composition of 0.1% ^{54}Fe, 2.94% ^{56}Fe, 54.90% ^{57}Fe and 42.06% ^{58}Fe was added to samples in a 1:1 natural:spike ratio at least 12 h prior to pre-concentration. Samples were analyzed in medium resolution mode (MR) to resolve polyatomic interferences, using the older Thermo MR slits (30 μm), which correspond more closely to the newer HR slits (18–25 μm). Isobaric interferences on ^{54}Fe and ^{58}Fe were corrected for using the measured abundances of ^{53}Cr and ^{60}Ni.

As described by Lacan et al. (2010), each analytical session began with analysis of the in-house ETH Zürich hematite standard relative to IRMM-014 (both mixed with the double-spike), and then the hematite standard was analyzed after every two samples as a check on accuracy and precision of the instrument. Each sample was bracketed by the blank acid, with 25 cycles of 8.4 s for samples and standards and 10 cycles of 8.4 s for blanks. This method has been shown to give excellent precision and accuracy over the full range of expected Fe concentrations in seawater (0.05–1 nmol kg^{-1}) in volumes of 2–20 L, with full details described previously (Lacan et al., 2010). Final values are either means calculated from multiple Neptune analysis of a single 10 L sample, calculated from separate extractions of 5 L aliquots, or a combination of the two. 2σ uncertainty on measurements is expressed as the long term reproducibility of the ETH Zürich standard (0.07‰), as the repeatability from seawater samples yielded better results (2σ from 0.01 to 0.05‰). Fe concentration measurements were made by isotope dilution, with a procedural blank corresponding to 0.002 nmol kg^{-1} and uncertainty is expressed as 2SD of replicate analyses (Lacan et al., 2010).

3. Results and discussion

The δ^{56}Fe and Fe data discussed in this study are reproduced from other interpretive studies (Abadie et al., in review; Boyle et al., 2012; Conway and John, 2014a; John and Adkins, 2012; Lacan et al., 2008), with the exception of GA10 results, which are presented here for the first time. All data shown in figures are available as Suppl. data.

3.1. GA03 (2011) and IC1 at Bermuda (2008)

The water column profiles of Fe and δ^{56}Fe for the BATS station from the IC1 and GA03 cruises are shown in Fig 2b, with the δ^{56}Fe values for the IC1 intercomparison depths shown in Fig. 2c–d. Good agreement within error was previously observed between the labs taking part in the IC1 cruise in these samples, for the GSI surface (7 m; Fig. 2c) and GDI deep tanks (2000 m; Fig. 2d), with δ^{56}Fe ranging from +0.24 ± 0.10‰ to +0.41 ± 0.04‰ for the surface tank and +0.42 ± 0.11‰ to +0.52 ± 0.07‰ for the deep tank (Boyle et al., 2012, see Suppl. data). All labs reported data within 2SD of the mean of the five labs (GSI +0.34 ± 0.13‰ and GSD +0.48 ± 0.10‰; 2SD), demonstrating the ability of the individual labs to accurately measure δ^{56}Fe at dissolved Fe concentrations of 0.4 and 0.8 nmol kg^{-1}.

For comparison of the IC1 and GA03 cruise, although samples were not taken at exactly the same depth, we can compare samples of similar depth (Fig 2c–d). At the surface, the GA03 towed fish sample (~2 m) is within 2SD of the mean δ^{56}Fe of the GSI tank (+0.23 ± 0.07‰ and +0.34 ± 0.13‰; Fig. 2c), and Fe concentrations show similar good agreement (0.46 vs. 0.41–0.45 nmol kg^{-1}). For the deep ocean, the GA03 samples collected at 1951 and 2101 m are also both within error of 2SD of the mean δ^{56}Fe of the GDI tank (+0.35 ± 0.06‰, +0.43 ± 0.07‰ and +0.48 ± 0.10‰; Fig. 2d), and the δ^{56}Fe of the GA03 sample at 2101 m is identical within error to the GSD Tank mean δ^{56}Fe. Fe concentrations measured for this depth interval on the GA03 cruise (0.61–0.65 nmol kg^{-1}) were slightly lower than those for the GSD tank (0.74–0.84 nmol kg^{-1}). Very similar temperature, oxygen and salinity profiles are also observed between the cruises, suggesting consistent water mass structure (Fig. 2b); despite this, given the dynamic nature of the marine Fe cycle, such consistency in δ^{56}Fe at both depths from the two cruises is remarkable. This is especially remarkable for the surface ocean in different seasons (June and November), three years apart, when this region of the ocean is prone to episodic

Fig. 3. Comparison of δ^{56}Fe and Fe profiles from GA03 Station USGT10–12 and USGT11–24 (17.4°N 24.5°W) from the Tenatso Time Series station in the North East Atlantic. a) Regional location map showing GA03 stations sampled for Fe isotope ratios. Dissolved Fe concentration (nmol kg^{-1}), dissolved δ^{56}Fe (relative to IRRM-014) and oceanographic parameters shown against depth (b) or σ$_\theta$ density (c). Data and 2σ error bars are from Conway and John (2014a). Temperature and salinity are from the GEOTRACES rosette and dissolved oxygen is from the ODF rosette. The shaded below denotes the influence of the Mauritanian Oxygen Minimum Zone (OMZ; dissolved oxygen < 120 μmol kg^{-1}).
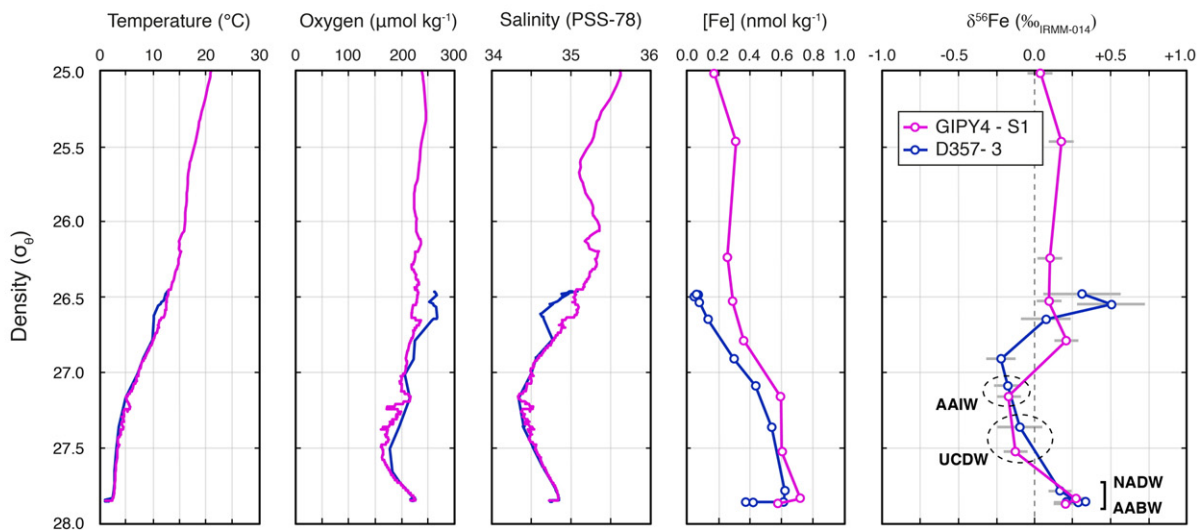
a) Location Map
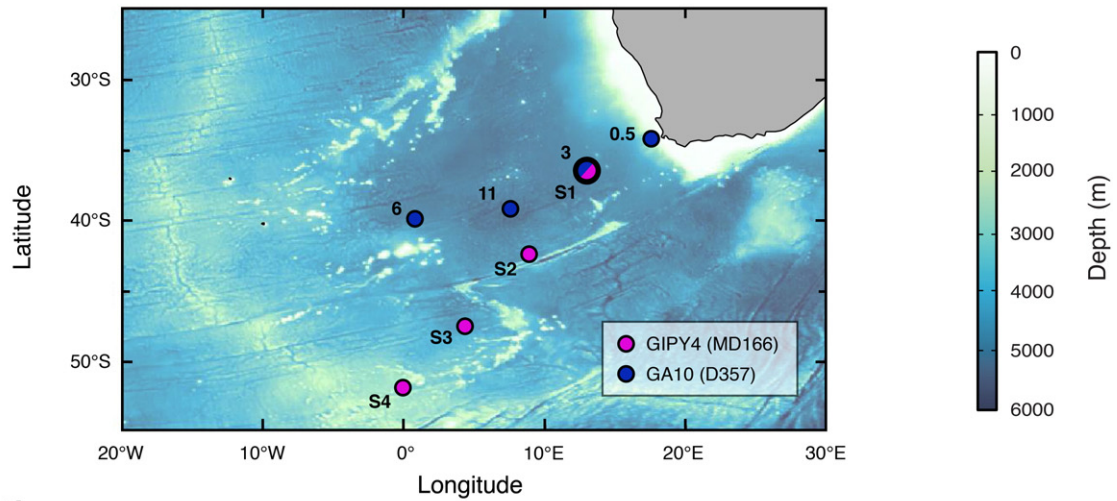
b) vs. Depth
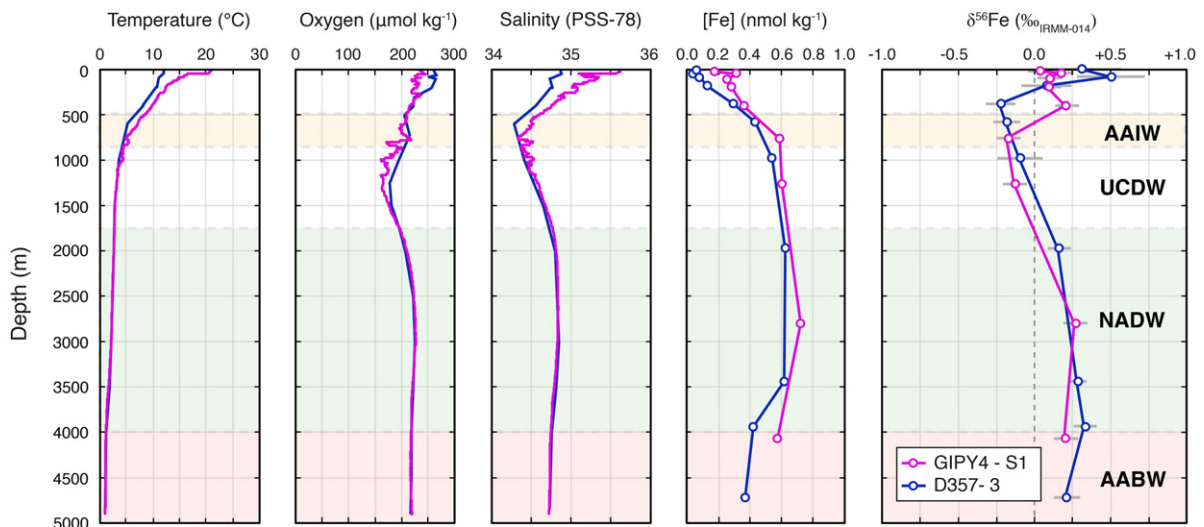
c) vs. Density

atmospheric supply of Fe with both storm activity and seasonality causing variability in the deposition of more-soluble anthropogenic aerosol Fe vs. lower-solubility lithogenic aerosol Fe (e.g. Fishwick et al., 2014; Sedwick et al., 2005; Sedwick et al., 2007; Wu and Boyle, 2002).

A lack of variability may in fact point to the stability of the Fe cycle in this region on this timescale in terms of overall Fe sources and internal cycling processes such as scavenging and biological uptake/release. Since anthropogenic and lithogenic aerosols might be expected to alternately dominate deposition in winter and summer respectively and have been suggested to have different δ^{56}Fe signatures (Conway, T. M., unpublished data; Fishwick et al., 2014; Mead et al., 2013; Sedwick et al., 2005), it is perhaps surprising that there is such little variability in surface water dissolved δ^{56}Fe. However, since the surface of neither profile is characterized by the very high Fe concentrations that have been attributed to episodes of lithogenic dust deposition in summer months (1–2 nmol kg^{-1}; Sedwick et al., 2005), it may be that both profiles reflect the longer-timescale combined effect of different Fe sources, equilibrium and kinetic processes in concert with dust particles rather than the primary δ^{56}Fe signature of each dust source. We previously suggested that the heavy δ^{56}Fe signature might represent an equilibrium effect of dust particles being in contact with organic ligands (Conway and John, 2014a), with the exchange/dissolution process in the presence of ligands perhaps ultimately more important than the δ^{56}Fe signature of either lithogenic or anthropogenic aerosols. However, this remains a hypothesis and clearly more process and experimental studies will be required to fully test this and to understand what is ultimately responsible for heavier-than-crustal δ^{56}Fe in surface Atlantic waters. As such, we cannot presently assess on the basis of these datasets whether episodic dust fluxes might cause dramatic effects on surface ocean dissolved δ^{56}Fe, perturbing the profiles observed here, or whether the magnitude of local dust flux has a negligible effect on δ^{56}Fe because the surface ocean δ^{56}Fe in this region is typically dominated by an internal cycling process.

Higher resolution comparison of δ^{56}Fe at BATS through the water column is also possible because of the measurement of a 10 point δ^{56}Fe profile on IC1 samples by Caltech (John and Adkins, 2012; Boyle et al., 2012), and a 34 point profile for δ^{56}Fe measured on samples from the GA03 cruise (Conway and John, 2014a). A general homogeneity of δ^{56}Fe through the full water column (+0.32‰ to +0.55‰ with one exception; Fig. 2b) for the IC1 samples was previously commented upon by John and Adkins (2012), who attributed heavy δ^{56}Fe to dust and the homogeneity to buffering of the dissolved phase by particles. They also attributed one exceptionally heavy δ^{56}Fe value (+0.78 ± 0.07‰) at 2500 m to a hydrothermal source. However, further study has called into question whether the heavy δ^{56}Fe value at 2500 m (bracketed point, Fig. 2b) was representative of the ocean. While the heavy δ^{56}Fe value reported by John and Adkins (2012) was confirmed by analyses at USC, this sample had anomalously low Zn and Cd concentrations, poor reproducibility of Fe concentration, and unexpectedly light δ^{66}Zn in this sample, compared to the typically homogenous deep ocean δ^{66}Zn value (−0.1 vs. +0.5‰; Conway and John, 2014b; Conway and John, 2015a; Conway et al., 2013a,b; Zhao et al., 2014). These lines of evidence suggest that the sample is likely not representative of 2500 m seawater, but rather that the Go-Flo bottle probably tripped at the wrong depth. Additional analysis of δ^{56}Fe for the whole IC1 profile from the same sample bottles at USC showed good overall agreement, within 2σ quoted uncertainty for most depths (Fig. 2b; Conway et al., 2013a,b, Suppl. information). However, it is worth noting that at 1500 m, δ^{56}Fe measurements from USC and Caltech were slightly

greater (0.13‰) than the combined 2σ uncertainty (0.12‰) apart, and that, while typically within 2σ uncertainty, the USC δ^{56}Fe dataset was generally heavier than Caltech by ~0.1‰. These differences could point to a slight underestimation of true analytical uncertainty by one or other of the methods, or some effect of 5 years of sample storage.

A similar broad homogeneity in δ^{56}Fe through the water column to that observed on IC1 was reported for BATS from the GA03 cruise, with δ^{56}Fe varying from +0.22 to +0.58‰, with the exception of one data point at 420 m (+0.7‰). Upon direct comparison of δ^{56}Fe data from the two cruises we observe very similar δ^{56}Fe profile shapes (Fig. 2b); in fact, with the exception of the IC1 samples at 250 m and 500 m (where we have no direct comparison between cruises) and 2500 m (the flagged sample), δ^{56}Fe from the other 7 depths from the Caltech IC1 cruise agree well with their depth counterparts from GA03, extending the observation of consistent δ^{56}Fe in GSI and GSD samples with GA03 to the full depth profile. While most USC IC1 cruise data also agree well with GA03 within 2σ uncertainty, the previously mentioned δ^{56}Fe data point at 1500 m appears to be slightly anomalously heavy compared to the other two datasets, and the USC IC1 value at 4200 m (+0.45 ± 0.06‰) is also slightly outside of 2σ internal uncertainty of GA03 (+0.29 ± 0.06‰), while agreeing with Caltech (+0.35 ± 0.07‰). These differences could also point to small variability between datasets, whether from natural variability, sampling contamination or a slight underestimation of true analytical uncertainty. Nevertheless, the overall agreement of the three datasets is strong, agreeing within ~0.1‰, and so differing by much smaller amounts than the range of variability observed elsewhere in the ocean (e.g. Fig 2–4).

The higher resolution of the GA03 profile compared to IC1 permits the observation of systematic variability in the deep ocean, with depth intervals where δ^{56}Fe ≤ +0.3‰ (800–1800 m and >3600 m) and > +0.3‰ between 1800 and 3600 m, corresponding to the influence of Upper Labrador Seawater and deep nepheloid layers respectively (Jenkins et al., 2015; Ohnemus and Lam, 2015), and attributed to the influence of a (non-reductive) sedimentary Fe source (Conway and John, 2014a). While the presence of similar δ^{56}Fe structure cannot be assessed for IC1 due to the depth resolution, the consistency of the full water column profile between the cruises does suggest that the broad external source addition and internal cycling processes that determine dissolved δ^{56}Fe throughout the water column in this region are likely to be similar at both times.

In terms of dissolved Fe concentration, the profiles for both cruises are very similar above 1500 m (Fig. 2a), including a surface enrichment (~0.4–0.5 nmol kg^{-1}) and pronounced dissolved Fe minimum at 120–140 m (0.1–0.2 nmol kg^{-1}) in both cruises. Below 1500 m, Fe concentrations were slightly higher on the IC1 cruise (0.1–0.2 nmol kg^{-1}) at the two comparable depths.

3.2. GA03 (2010 and 2011) at Cape Verde

The GA03 section was completed on two cruises in 2010 and 2011, with station identification defined as USGT, then 10 or 11 for year, then station number (e.g. USGT10–12). The cruises overlapped with re-occupation of the Tenatso Time Series station (17.40°N 24.50°W) near Cape Verde by the GA03 cruise in Oct. 2010 (USGT10–12) and Nov. 2011 (USGT11–24). Depth and density profiles of dissolved δ^{56}Fe and Fe are shown for these two stations in Fig. 3b–c.

Both occupations at the Tenatso Time Series station were characterized by very similar temperature, salinity and oxygen vertical profiles on both density and depth scales, with oxygen slightly higher in 2010

Fig. 4. Comparison of δ^{56}Fe and Fe profiles from Superstation 3 of GA10 D357 cruise and Super-Station 1 (station 18) of GIPY4 cruise in the South East Atlantic. a) Regional location map showing GIPY4 and GA10 stations sampled for Fe isotope ratios. Dissolved Fe concentration (nmol kg^{-1}) and dissolved δ^{56}Fe (relative to IRRM-014) shown against depth (b) or σ_θ density (c). Data are from Abadie et al. (in review), Lacan et al. (2008), or previously unpublished. Error bars are 2σ as described in the text. GA10 temperature and salinity are from the titanium rosette and oxygen from the stainless steel rosette, corrected to match bottle measurements. GIPY temperature, salinity and oxygen data are from the Niskin Rosette. The horizontal shaded bars represent the presence of different water masses based on salinity (see text; Antarctic Intermediate Water, AAIW; Upper Circumpolar Deep Water, UCDW; North Atlantic Deep Water, NADW; Antarctic Bottom Water, AABW). N.B. The position of AAIW in depth space is based on GA10 and was deeper for GIPY4.

(Fig. 3b–c). The vertical structure is strongly dominated by the Mauritanian Oxygen Minimum Zone (OMZ) present between ~200 and 1000 m, with dissolved oxygen as low as 60 μmol kg^{-1}, as well as a very shallow mixed layer (~40–50 m; Hatta et al., 2015). The dissolved Fe concentration profiles for both stations reflect this vertical structure, with both showing a surface enrichment of 0.3–0.4 nmol kg^{-1} in the mixed layer, presumably from atmospheric dust, a dissolved Fe minimum of 0.1–0.2 nmol kg^{-1} just below the mixed layer (associated with the fluorescence maximum; 60–70 m), elevated concentrations of 0.8–1.2 nmol kg^{-1} through the OMZ horizon, and Fe concentrations declining to 0.6 nmol kg^{-1} in the deep ocean (Conway and John, 2014a; Fig. 3b). Although dissolved Fe profiles from both years show very similar overall shapes, and strong consistency in waters >1000 m, there is some apparent variability within surface waters and especially throughout the OMZ horizon (Fig. 3b), a feature also reported by other investigators reporting dissolved Fe, Fe-binding ligands, Fe size fractionation and other parameters such as Pb concentrations and Cd isotopes on GA03 (Buck et al., 2015; Conway and John, 2014a, 2015b; Fitzsimmons et al., 2015; Hatta et al., 2015; Noble et al., 2015). Potential interannual variability is discussed in the context of δ^{56}Fe later in this section.

δ^{56}Fe measurements through the water column at this location show greater variability in a single profile than at the BATS station (Section 3.1), with both USGT10–12 and USGT11–24 spanning a range of 0.7‰ (between 0 and +0.7‰). Similar to the consistency in dissolved Fe concentrations, the δ^{56}Fe profiles for both years are broadly similar in shape, with heavy δ^{56}Fe values within the mixed layer (>+0.4‰), a sub-surface minimum (0‰), values of 0 to +0.3 ‰ within the OMZ region, and values increasing from +0.2 to as high as +0.7‰ in deep water, as Fe concentrations decline (Fig. 3b). This structure was previously attributed to isotopically heavy Fe released from dust (+0.7‰) in the surface mixed layer and the deep ocean, mixing with a reductive sediment light Fe (<−1‰) that is transported throughout the water column (but mostly within OMZ waters) from reducing sediments on the Mauritanian margin (Conway and John, 2014a).

Samples were collected at the same depth on each cruise, allowing direct comparison of δ^{56}Fe values for each profile. For the surface dissolved Fe enrichment in the mixed layer, δ^{56}Fe values were very similar between cruises (2–50 m; +0.52 ± 0.09‰ and +0.41 ± 0.09‰ in 2010, +0.60 ± 0.09‰, +0.60 ± 0.09‰, and +0.63 ± 0.09‰ in 2011; Fig. 3b). In density space, these surface values show poorer agreement (Fig. 3c), perhaps due to changes in the relative importance of North Atlantic Central Water or Atlantic Equatorial Water between the two years (Hatta et al., 2015; Jenkins et al., 2015). However, if isotopically heavy values result from local dissolution of sinking dust in surface waters, then variability in vertical density may not be an appropriate parameter for comparison. Below the mixed layer, from 70 to 240 m depth, the two profiles are equivalent within error for δ^{56}Fe, with δ^{56}Fe values of +0.2‰ associated with both the subsurface dissolved Fe concentration minimum and fluorescent maximum, as well as a δ^{56}Fe minimum of 0.0‰ just below the Fe minimum, as Fe concentrations begin to rise. While it is not yet clear what processes (such as regeneration, uptake or scavenging) cause this intriguing subsurface structure, it is reproduced for both years here, and was also observed associated with the Fe minimum in other nearby GA03 profiles (Conway and John, 2014a). Surface variability in the top 300 m may be induced by not only changes in atmospheric dust deposition and biological processes, but also in the relative importance of different surface water masses with different characteristics, so it is notable that Fe and δ^{56}Fe are so consistent at shallow depths.

Set against the broad similar δ^{56}Fe profile shapes, there is poorer agreement between δ^{56}Fe depth pairs throughout both the OMZ horizon and the (ocean deeper than 200 m). With the exception of δ^{56}Fe data from 3198 m, the δ^{56}Fe profile from 2011 is notably isotopically heavier than that of 2010 (by 0.03 to 0.3‰). While some of these differences (8 of the 17 depths) are within combined 2σ uncertainty

(≥0.10‰), some are larger (Fig. 3b; Suppl. data). Indeed, throughout the OMZ horizon (~200–1000 m; shown as a blue bar in Fig 3b), where most of the Fe concentration measurements are different between the two cruises (by 0.1 to 0.2 nmol kg^{-1}), four of the seven δ^{56}Fe data points are outside of error of each other. Deeper in the ocean (below 1000 m), where Fe concentrations show strong consistency, δ^{56}Fe show variability between the cruises, identical within error between 1000 and 1300 m, 2000–2300 and >3000 m, but differing between 1500 and 1750 and 2500–3000 m. While Fe concentrations are consistent for most of these depths (differing by < 0.02 nmol kg^{-1}, similar to expressed error of 0.01–0.02 nmol kg^{-1}), the largest differences in δ^{56}Fe in this interval (0.19‰ and 0.26‰ at 1500 and 2748 m respectively) are found at depths where Fe concentrations are subtly more different (0.06–0.1 nmol kg^{-1}). Thus, while it is possible that some of this variability in δ^{56}Fe in the deep ocean represents differences in background contamination or underestimation of δ^{56}Fe analytical uncertainty, especially when it is not accompanied by changes in Fe concentration, it is consistent with observed variability in other oceanographic parameters. Variability in Fe cycling would also not be unexpected, given the dynamic oceanographic nature of this region. Upwelling of nutrient and Fe rich deep water, high productivity in surface waters, an OMZ at intermediate depths facilitating potential advection of shelf Fe, and the presence of Antarctic water masses at intermediate depths could all lead to variability in Fe cycling and hence δ^{56}Fe signatures.

Variability in δ^{56}Fe and Fe in the deep ocean is also consistent with the idea that dissolved Fe in this region is dominantly locally sourced from atmospheric dust or reductive sediments that have very different δ^{56}Fe signatures (Conway and John, 2014a). Thus, small changes in either sediment or dust supply could dramatically influence δ^{56}Fe, while having only a small effect on Fe concentrations. A shelf source of Fe might be expected to have a waning influence with distance from Africa, as well as varying with strength over time, while dust supply would also be episodic and seasonal. If we examine data from stations USGT10–12 and 11–24 in the context of nearby stations (USGT10–11 and USGT11–24; Fig. 3a; Suppl. Fig. S1), it can be observed that USGT11–22, a 2011 station further from Africa (Fig. 3a), is characterized by much lower Fe concentrations throughout the water column as well as generally heavier δ^{56}Fe, while USGT10–11, a 2010 station nearer to Africa, is practically identically to USGT10–12 for δ^{56}Fe below 500 m. Given that USGT11–24 looks more similar to USGT11–22 below 800 m within the depth intervals at which USGT10–12 and USGT11–24 disagree (lower Fe concentrations and higher δ^{56}Fe), it is possible to interpret the full water-column variability as being driven by a changing component of isotopically light Fe from reductive sediments that is slightly greater in 2011 than 2010. At shallower depths (286–451 m), USGT11–24 is characterized by higher Fe concentrations and heavier δ^{56}Fe than both USGT10–11 and USGT10–12, as well as slightly lower oxygen (Suppl. Fig. S1; Fig. 3b; Hatta et al., 2015); thus, this difference could not be explained by an increased source of light Fe in 2011, but perhaps rather by a greater dissolution of atmospheric dust or regeneration of Fe within the OMZ.

3.3. GIPY4 (2008) and GA10 (2010)

Water-column profiles of dissolved δ^{56}Fe and Fe for and GIPY4 Super-Station S1 (2008) and GA10 D357 Station 3 (2010) from the Cape Basin in the Eastern South Atlantic are shown together with supporting oceanographic parameters, plotted against both depth and density in Fig. 4. Below 700 m, similar temperature, oxygen and salinity profiles are observed for both cruises, while in surface waters the GIPY4 cruise was characterized by much warmer, fresher, less dense water than GA10 (Fig. 4b–c). This difference can be most clearly observed in density space for σ$_θ$ > 26.75 kg m^{-3} (Fig. 4c), indicative of different surface waters dominating the upper water column (< 700 m) during the two cruises. This difference could be due to movement in the position

of the South Subtropical Convergence, which is located near this station (Fig. 1 of Browning et al., 2014), and/or the variable influence of the Agulhas current, which variably transports warm salty surface water from the Indian Ocean to the South Atlantic within mesoscale structures (Lutjeharms, 2006). Indian ocean water is transported into the Atlantic within the Agulhas retroflection, typically in the form of large anticyclonic eddies ('Agulhas rings'; Lutjeharms, 2006). Such rings, characterized both on the GA10 and GIPY4 cruises by elevated temperature, salinity and nutrients (S > 35; T 15–23 °C; Arhan et al., 2011; Wyatt et al., 2014), can have an important effect on both biogeochemical cycling in surface waters (Villar et al., 2015); indeed, it was recently shown that Agulhas rings transport an Indian Ocean Pb isotope signature to the North Atlantic (Paul et al., 2015), suggesting that they could also play a role in influencing the surface ocean cycling of Fe and other trace metals.

The difference in surface water characteristics is also reflected in the Fe concentration profiles, which show broad similarity for both cruises below 400 m, but disagreement in surface waters < 100 m where dissolved Fe was 0.2–0.3 nmol kg^{-1} in 2008 and < 0.09 nmol kg^{-1} in 2010, perhaps due to the transport of higher Fe concentrations within warmer saltier Indian Ocean water compared to colder more-Fe depleted Atlantic waters. As might be expected, with the surface variability in surface waters and Fe concentrations, δ^{56}Fe between the cruises show differences between the two cruises (Fig. 4b); δ^{56}Fe from GIPY4 are rather homogenous over the top 400 m, and close to crustal (+0.09‰; Beard et al., 2003; Lacan et al., 2008), varying only between +0.04 ± 0.07‰ and +0.21 ± 0.07‰. In contrast, although subject to larger uncertainties at low surface Fe concentrations, δ^{56}Fe from GA10 show more variability in the top 500 m, ranging from −0.22 ± 0.10‰ to +0.51 ± 0.22‰. When compared in density space (Fig. 4c), it becomes clear that much of the GIPY4 data are from lower density waters; this, together with the documented agreement of data from the two labs at BATS (Section 3.1) and in the deep ocean at this location (see below), suggests that this variability in δ^{56}Fe may be natural rather than analytical and could perhaps also be attributed to the greater influence of Indian Ocean water in 2008. Although to date no δ^{56}Fe data has been reported from the Indian Ocean, the near-crustal homogenous δ^{56}Fe in Indian Ocean water above 400 m could reflect non-reductive release of Fe from sediments as suggested in the Equatorial Pacific and North Atlantic Oceans (Radic et al., 2011; Conway and John, 2014a; Labatut et al., 2014) and observed in situ within sediment pore waters (Homoky et al., 2013).

In terms of the ocean below ~500 m, the South Atlantic at this location is dominated by the lateral South–North or North–South movement of Southern- and Northern-sourced water masses, especially for nutrients and trace metals such as Zn (Wyatt et al., 2014). The depth intervals of these water masses, specifically Antarctic Intermediate Water (AAIW), Upper Circumpolar Deep Water (UCDW), North Atlantic Deep Water (NADW), and Antarctic Bottom Water (AABW), are shown in Fig. 4b–c, and are defined following Wyatt et al. (2014), based either on salinity, with NADW >34.75 (~1700–4000 m) and AAIW <34.4. For δ^{56}Fe below 700 m, the two δ^{56}Fe profiles are identical within 2σ uncertainty (Fig. 4b). Above this, between 500 and 700 m, although there are no direct comparable samples, there appears to be a disagreement in δ^{56}Fe. However, for comparison purposes it is important to note that the salinity minimum corresponding to AAIW was from ~500–950 m for GA10 (as shown in Fig. 4b), but deeper (750–950 m) for GIPY4, suggesting that the isotopically light δ^{56}Fe of −0.18 ± 0.09‰ at 594 m from GA10 is in fact most comparable to the −0.17 ± 0.07‰ at 763 m from GIPY4; this can be seen more clearly in density space (Fig. 4c). With this adjustment in mind, δ^{56}Fe can be considered identical within uncertainty for both cruises over the entire water column below 500 m. This remarkable consistency in water-column δ^{56}Fe, in contrast to surface waters at this location, highlights the quality of data being produced by both laboratories, as well as again pointing to the stability of Fe sources and cycling in the ocean at this location on this timescale, similar to that suggested at Bermuda.

Little temporal variability on this timescale suggests that the deep water masses at this location may have relatively stable transported δ^{56}Fe signatures, similar to that observed in the Western North Atlantic (Section 3.1). Such signatures can be observed when water mass horizons are shown on the δ^{56}Fe profile (Fig. 4b), with AABW (+0.21 ± 0.07‰, and +0.21 ± 0.09‰) slightly isotopically heavier than crustal, NADW (+0.29 ± 0.06‰, +0.33 ± 0.07, and +0.27 ± 0.07‰) distinctly isotopically heavier than crustal, while UCDW (−0.12 ± 0.07‰ and −0.09 ± 0.15‰) and AAIW (−0.17 ± 0.07‰ and −0.18 ± 0.09‰) are both isotopically light. One additional GA10 sample from 2000 m, from shallower depths of NADW, was slightly lighter (+0.17 ± 0.08‰), perhaps reflecting mixing with the above-lying isotopically lighter UCDW. While it is not clear what might cause these differences in water mass δ^{56}Fe signatures, it could point to δ^{56}Fe retained from different dominant Fe sources (e.g. reductive versus non-reductive sediment dissolution), or to fractionation processes during formation or transport of these water masses. These ideas are explored in greater detail in the context of the full GIPY4 section in Abadie et al. (in review).

4. Conclusions

We have presented the first oceanic comparison of dissolved δ^{56}Fe depth profiles from three locations in the Atlantic Ocean, including both the first full profile interlaboratory comparison and comparison with a previous intercalibration exercise. We found that: (1) There is strong agreement between data and profiles produced by the two laboratories compared in this study, and the five laboratories compared in the previous exercise, which allows the combination and interpretation of δ^{56}Fe datasets from different laboratories. Where discrepancies exist between laboratories, they are typically on the order of 0.1‰, which is occasionally greater than stated analytical uncertainty, but much less than the overall variability in δ^{56}Fe observed within the global ocean. While some of this discrepancy may be due to true analytical error or sample storage/handling, our data suggest that variability between cruises may also be driven by true natural variability in δ^{56}Fe. Thus, repeat occupation of oceanic stations by different GEOTRACES cruises and δ^{56}Fe analysis by different laboratories is essential for continued evaluation and comparison of analytical methods, but also permits evaluation of temporal variability in oceanic Fe cycling. (2) At all three locations compared in this study, there was remarkable agreement in the overall shape of δ^{56}Fe profiles on a 1–3 year timescale, including almost complete agreement over the full water column at Bermuda in the Western North Atlantic and for the water column below 500 m in the South Atlantic. (3) Set against this overall homogeneity in δ^{56}Fe, we observe apparent natural variability in δ^{56}Fe in shallow waters in the South Atlantic, and throughout the water column in the Eastern subtropical North Atlantic, close to North Africa. Overall, where δ^{56}Fe invariance is observed, we suggest that the internal cycling and sources of δ^{56}Fe is stable on these timescales, in regions of the oceans dominated by stable water-masses or single Fe sources (e.g. atmospheric dust). However, δ^{56}Fe may be more dynamic in surface waters with variable currents, upwelling/regeneration or low-oxygen waters, all of which may either facilitate the supply of Fe from different sources with different δ^{56}Fe signatures or faciliate changes in the internal cycling of Fe. Taken together, this work lends weight to the use of δ^{56}Fe as a tracer to increase our understanding of the variability in supply from different Fe sources and transport of Fe through the oceans, or in internal Fe cycling.

Supplementary data to this article can be found online at http://dx.doi.org/10.1016/j.marchem.2016.04.007.

References

Abadie, C. Lacan, F., Radic, A., Pradoux, C., Poitrasson, F. In review. Iron isotopes reveal distinct dissolved iron sources and pathways in the intermediate versus deep Southern Ocean. Proc. Natl Acad. Sci. USA.

Anderson, R.F., Henderson, G.M., 2005. GEOTRACES a global study of the marine biogeochemical cycles of trace elements and their isotopes. Oceanography 18, 76–79. http://dx.doi.org/10.5670/oceanog.2005.31.

Arhan, M., Speich, S., Messager, C., Dencausse, G., Fine, R., Boye, M., 2011. Anticyclonic and cyclonic eddies of subtropical origin in the subantartic zone south of Africa. J. Geophys. Res. 116, C11. http://dx.doi.org/10.1029/2011JC007140.

Beard, B.L., Johnson, C.M., Von Damm, K.L., Poulson, R.L., 2003. Iron isotope constraints on Fe cycling and mass balance in oxygenated Earth oceans. Geology 31, 629–632. http://dx.doi.org/10.1130/0091-7613(2003)031<0629:IICOFC>2.0.CO;2.

Boyle, E.A., John, S.G., Abouchami, W., Adkins, J.F., Echegoyen-Sanz, Y., Ellwood, M.J., Flegal, A.R., Fornace, K., Gallon, C., Galer, S., Gault-Ringold, M., Lacan, F., Radic, A., Rehkämper, M., Rouxel, O., Sohrin, Y., Stirling, C., Thompson, C., Vance, D., Xue, Z., Yhao, Y., 2012. GEOTRACES IC1 (BATS) contamination-prone trace element isotopes Cd, Fe, Pb, Zn, Cu, and Mo intercalibration. Limnol. Oceanogr. Methods 10, 653–665. http://dx.doi.org/10.4319/lom.2012.10.653.

Browning, T.J., Bouman, H.A., Moore, C.M., Schlosser, C., Tarran, G.A., Woodward, E.M.S., Henderson, G.M., 2014. Nutrient regimes control phytoplankton ecophysiology in the South Atlantic. Biogeosciences 11, 463–479. http://dx.doi.org/10.5194/bg-11-463-2014.

Buck, K.N., Sohst, B., Sedwick, P.N., 2015. The organic complexation of dissolved iron along the U.S. GEOTRACES (GA03) North Atlantic Section. Deep-Sea Res. II Top. Stud. Oceanogr. 116, 152–165. http://dx.doi.org/10.1016/j.dsr2.2014.11.016.

Chever, F., Rouxel, O.J., Croot, P.L., Ponzevera, E., Wuttig, K., Auro, M., 2015. Total dissolvable and dissolved iron isotopes in the water column of the Peru upwelling regime. Geochim. Cosmochim. Acta 162, 66–82. http://dx.doi.org/10.1016/j.gca.2015.04.031.

Conway, T.M., John, S.G., 2014a. Quantification of dissolved iron sources to the North Atlantic Ocean. Nature 511, 212–215. http://dx.doi.org/10.1038/nature13482.

Conway, T.M., John, S.G., 2014b. The biogeochemical cycling of zinc and zinc isotopes in the North Atlantic Ocean. Glob. Biogeochem. Cycles 28, 1111–1128. http://dx.doi.org/10.1002/2014GB004862.

Conway, T.M., John, S.G., 2015a. The cycling of iron, zinc and cadmium in the North East Pacific Ocean — insights from stable isotopes. Geochim. Cosmochim. Acta 164 (1), 262–283. http://dx.doi.org/10.1016/j.gca.2015.05.023.

Conway, T.M., John, S.G., 2015b. Biogeochemical cycling of cadmium isotopes along a high-resolution section through the North Atlantic Ocean. Geochim. Cosmochim. Acta 148, 269–283. http://dx.doi.org/10.1016/j.gca.2014.09.032.

Conway, T.M., Rosenberg, A.D., Adkins, J.F., John, S.G., 2013a. A new method for precise determination of iron, zinc and cadmium stable isotope ratios in seawater by double-spike mass spectrometry. Anal. Chim. Acta 793, 44–52. http://dx.doi.org/10.1016/j.aca.2013.07.025.

Conway, T.M., Rosenberg, A.D., Adkins, J.F., John, S.G., 2013b. Corrigendum to "A new method for precise determination of iron, zinc and cadmium stable isotope ratios in seawater by double-spike mass spectrometry." [Anal. Chim. Acta 793, 44–52]. Anal. Chim. Acta 801 (97). http://dx.doi.org/10.1016/j.aca.2013.09.010.

Cutter, G., Andersson, P. Codispoti, L. Croot, P., François, R., Lohan, M. C., Obata, H., Rutgers van der Loeff, M., 2010. Sampling and Sample-handling Protocols for GEOTRACES Cruises. Version 1.0, December 2010, http://www.geotraces.org/images/stories/documents/intercalibration/Cookbook_v1_2010.pdf

Cutter, G.A., 2013. Intercalibration in chemical oceanography—getting the right number. Limnol. Oceanogr. Methods 11, 418–424. http://dx.doi.org/10.4319/lom.2013.11.418.

Cutter, G.A., Bruland, K.W., 2012. Rapid and noncontaminating sampling system for trace elements in global ocean surveys. Limnol. Oceanogr. Methods 10 (6), 425–436. http://dx.doi.org/10.4319/lom.2012.10.425.

Cutter, G., Andersson, P. Codispoti, L. Croot, P., François, R., Lohan, M. C., Obata, H., Rutgers van der Loeff, M., 2014. Sampling and Sample-handling Protocols for GEOTRACES Cruises. Version 2.0, December 2014, http://www.geotraces.org/images/stories/documents/intercalibration/Cookbook.pdf

de Jong, J., Schoemann, V., Tison, J.L., Becquevort, S., Masson, F., Lannuzel, D., Petit, J., Chou, L., Weiss, D., Mattielli, N., 2007. Precise measurement of Fe isotopes in marine

samples by multi-collector inductively coupled plasma mass spectrometry (MC-ICP-MS). Anal. Chim. Acta 589, 105–119. http://dx.doi.org/10.1016/j.aca.2007.02.055.

Ellwood, M.J., Hutchins, D.A., Lohan, M.C., Milne, A., Nasemann, P., Nodder, S.D., Sander, S.G., Strzepek, R., Wilhelm, S.W., Boyd, P.W., 2014. Iron stable isotopes track pelagic iron cycling during a subtropical phytoplankton bloom. Proc. Natl. Acad. Sci. U. S. A. 112, E15–E20. http://dx.doi.org/10.1073/pnas.1421576112.

Fishwick, M.P., Sedwick, P.N., Lohan, M.C., Worsfold, P.J., Buck, K.N., Church, T.M., Ussher, S.J., 2014. The impact of changing surface ocean conditions on the dissolution of aerosol iron. Glob. Biogeochem. Cycles 28 (11), 1235–1250. http://dx.doi.org/10.1002/2014GB004921.

Fitzsimmons, J.N., Carrasco, G.G., Wu, J.F., Roshan, S., Hatta, M., Measures, C.I., Conway, T.M., John, S.G., Boyle, E.A., 2015. Partitioning of dissolved iron and iron isotopes into soluble and colloidal phases along the U.S. GEOTRACES North Atlantic Transect. Deep Sea Res. Part II 116, 130–151. http://dx.doi.org/10.1016/j.dsr2.2014.11.014.

Hatta, M., Measures, C.I., Wu, J., Roshan, S., Fitzsimmons, J.N., Sedwick, P., Morton, P., 2015. An overview of dissolved Fe and Mn distributions during the 2010–2011 U.S. GEOTRACES North Atlantic cruises: GEOTRACES GA03. Deep Sea Res. Part II 116, 117–129. http://dx.doi.org/10.1016/j.dsr2.2014.07.005.

Henderson, G.M., Anderson, R.F., Adkins, J.F., Andersson, P., Boyle, E.A., Cutter, G., de Baar, H.J.W., Eisenhauer, A., Frank, M., Francois, R., Orians, K., Gamo, T., German, C.R., Jenkins, W.J., Moffett, J.W., Jeandel, C., Jickells, T.D., Krishnaswami, S., Mackey, D., Measures, C.I., Moore, J.K., Oschlies, A., Pollard, R., van der Loeff, M.R.D., Schlitzer, R., Sharma, M., von Damm, K., Zhang, J., Grp, S.W., 2007. GEOTRACES — an international study of the global marine biogeochemical cycles of trace elements and their isotopes. Chemie Der Erde-Geochemistry 67 (2), 85–131. http://dx.doi.org/10.1016/j.chemer.2007.02.001.

Homoky, W.B., John, S.G., Conway, T.M., Mills, R.A., 2013. Distinct iron isotope signatures and supply from marine sediment dissolution. Nat. Commun. 4, 2143. http://dx.doi.org/10.1038/ncomms3143.

Jenkins, W.J., Smethie, W., Boyle, E.A., Cutter, G.C., 2015. Water mass analysis for the U.S. GEOTRACES North Atlantic Sections. Deep Sea Res. Part II 116, 6–20. http://dx.doi.org/10.1016/j.dsr2.2014.11.018.

John, S.G., 2012. Optimizing sample and spike concentrations for isotopic analysis by double-spike ICPMS. J. Anal. At. Spectrom. 27, 2123–2131. http://dx.doi.org/10.1039/c2ja30215b.

John, S.G., Adkins, J.F., 2010. Analysis of dissolved iron isotopes in seawater. Mar. Chem. 119, 65–76. http://dx.doi.org/10.1016/j.marchem.2010.01.001.

John, S.G., Adkins, J.F., 2012. The vertical distribution of iron stable isotopes in the North Atlantic near Bermuda. Glob. Biogeochem. Cycles 26 (2). http://dx.doi.org/10.1029/2011GB004043.

John, S.G., Mendez, J., Moffett, J.W., Adkins, J.F., 2012. The flux of iron and iron isotopes from San Pedro Basin sediments. Geochim. Cosmochim. Acta 93, 14–29. http://dx.doi.org/10.1016/j.gca.2012.06.003.

Klunder, M.B., Laan, P., Middag, R., de Baar, H.J.W., Bakker, K., 2012. Dissolved iron in the Arctic Ocean: important role of hydrothermal sources, shelf input and scavenging removal. J. Geophys. Res. 117, C04014. http://dx.doi.org/10.1029/2011JC007135.

Labatut, M., Lacan, F., Pradoux, C., Chmeleff, J., Radic, A., Murray, J.W., Poitrasson, F., Johansen, A.M., Thil, F., 2014. Iron sources and dissolved-particulate interactions in the seawater of the Western Equatorial Pacific, iron isotope perspective. Glob. Biogeochem. Cycles 28, 1044–1065. http://dx.doi.org/10.1002/2014GB004928.

Lacan, F., Radic, A., Jeandel, C., Poitrasson, F., Sarthou, G., Pradoux, C., Freydier, R., 2008. Measurement of the isotopic composition of dissolved iron in the open ocean. Geophys. Res. Lett. 35, L24610. http://dx.doi.org/10.1029/2008GL035841.

Lacan, F., Radic, A., Labatut, M., Jeandel, C., Poitrasson, F., Sarthou, G., Pradoux, C., Chmeleff, J., Freydier, R., 2010. High-precision determination of the isotopic composition of dissolved iron in iron depleted seawater by double spike multicollector-ICPMS. Anal. Chem. 82, 7103–7111. http://dx.doi.org/10.1021/ac1002504.

Lutjeharms, E., 2006. The Agulhas Current. Springer Berlin Heidelberg, Berlin, Heidelberg.

Mawji, E., Schlitzer, R., Dodas, E.M., Abadie, C., Abouchami, W., Anderson, R.F., Baars, O., Bakker, K., Baskaran, M., Bates, N.R., Bluhm, K., Bowie, A., Bown, J., Boye, M., Boyle, E.A., Branellec, P., Bruland, K.W., Brzezinski, M., Bucciarelli, E., Buesseler, K., Butler, E., Cai, P., Cardinal, D., Casciotti, K., Chavez, J., Cheng, H., Chever, F., Church, T.M., Colman, A., Conway, T.M., Croot, P., Cutter, G., de Baar, H.J.W., de Souza, G., Dehairs, F., Deng, F., Dieu, H.T., Dulaquais, G., Echegoyen-Sanz, Y., Lawrence Edwards, R., Fahrbach, E., Fitzsimmons, J., Fleisher, M., Frank, M., Friedrich, J., Fripiat, F., Galer, S., Gamo, T., Solsona, E.G., Gerringa, L.J.A., Godoy, J., Gonzalez, S., Grossteffan, E., Hatta, M., Hayes, C.T., Heller, M.I., Henderson, G., Huang, K.-F., Jeandel, C., Jenkins, W.J., John, S., Kenna, T.C., Klunder, M., Kretschmer, S., Kumamoto, Y., Laan, P., Labatut, M., Lacan, F., Lam, P.J., Lannuzel, D., le Moigne, F., Lechtenfeld, O.J., Lohan, M., Lu, Y., Masqué, P., McClain, C.R., Measures, C., Middag, R., Moffett, J., Navidad, A., Nishioka, J., Noble, A., Obata, H., Ohnemus, D.C., Owens, S., Planchon, F., Pradoux, C., Puigcorbé, V., Quay, P., Radic, A., Rehkämper, M., Remenyi, T., Rijkenberg, M.J.A., Rintoul, S., Robinson, L.F., Roeske, T., Rosenberg, M., van der Loeff, M.R., Ryabenko, E., Saito, M.A., Roshan, S., Salt, L., Sarthou, G., Schauer, U., Scott, P., Sedwick, P.N., Sha, L., Shiller, A.M., Sigman, D., Smethie, W., Smith, G.J., Sohrin, Y., Speich, S., Stichel, T., Stutsman, J., Swift, J.H., Tagliabue, A., Thomas, A., Tsunogai, U., Twining, B.S., van Aken, H.M., van Heuven, S., van Ooijen, J., van Weerlee, E., Venchiarutti, C., Voelker, A.H.L., Wake, B., Warner, M.J., Woodward, E.M.S., Wu, J., Wyatt, N., Yoshikawa, H., Zheng, X., Xue, Z., Zieringer, M., Zimmer, L.A., 2015. The GEOTRACES intermediate data product 2014. Mar. Chem. 177 (1), 1–8. http://dx.doi.org/10.1016/j.marchem.2015.04.005.

Mead, C., Herckes, P., Majestic, B.J., Anbar, A.D., 2013. Source apportionment of aerosol iron in the marine environment using iron isotope analysis. Geophys. Res. Lett. 40 (21), 1944–8007. http://dx.doi.org/10.1002/2013GL057713.

Middag, R., Séférian, R., Conway, T.M., John, S.G., Bruland, K.W., de Baar, H.J.W., 2015. Intercomparison of dissolved trace elements at the Bermuda Atlantic time series

station. Mar. Chem. 177 (3), 476–479. http://dx.doi.org/10.1016/j.marchem.2015.06.014.

Moore, J.K., Doney, S.C., Glover, D.M., Fung, I.Y., 2001. Iron cycling and nutrient-limitation patterns in surface waters of the World Ocean. Deep-Sea Res. II Top. Stud. Oceanogr. 49, 463–507. http://dx.doi.org/10.1016/S0967-0645(01)00109-6.

Nishioka, J., Obata, H., Tsumune, D., 2013. Evidence of an extensive spread of hydrothermal dissolved iron in the Indian Ocean. Earth Planet. Sci. Lett. 361, 26–33. http://dx.doi.org/10.1016/j.epsl.2012.11.040.

Noble, A.E., Echegoyen-Sanz, Y., Boyle, E.A., Ohnemus, D.C., Lam, P.J., Kayser, R., Reuer, M., Wu, J., Smethie, W., 2015. Dynamic variability of dissolved Pb and Pb isotope composition from the U.S. North Atlantic GEOTRACES transect. Deep Sea Res. Part II 116, 208–225. http://dx.doi.org/10.1016/j.dsr2.2014.11.011.

Ohnemus, D.C., Lam, P.J., 2015. Cycling of lithogenic marine particulates in the US GEOTRACES North Atlantic transect. Deep-Sea Res. II Top. Stud. Oceanogr. 116, 283–302. http://dx.doi.org/10.1016/j.dsr2.2014.11.019.

Paul, M., van de Flierdt, T., Rehkämper, M., Khondoker, R., Weiss, D., Lohan, M.C., Homoky, W.B., 2015. Seawater lead isotopes trace Agulhas leakage. Geophys. Res. Lett. 42, 8515–8521. http://dx.doi.org/10.1002/2015GL065625.

Radic, A., Lacan, F., Murray, J.W., 2011. Iron isotopes in the seawater of the equatorial Pacific Ocean: new constraints for the oceanic iron cycle. Earth Planet. Sci. Lett. 306, 1–10. http://dx.doi.org/10.1016/j.epsl.2011.03.015.

Resing, J.A., Sedwick, P.N., German, C.R., Jenkins, W.J., Moffett, J.W., Sohst, B.M., Tagliabue, A., 2015. Basin-scale transport of hydrothermal dissolved metals across the South Pacific Ocean. Nature 523, 200–203. http://dx.doi.org/10.1038/nature14577.

Rijkenberg, M.J.A., Middag, R., Laan, P., Gerringa, L.J.A., van Aken, H.M., Schoemann, V., de Jong, J.T.M., de Baar, H.J.W., 2014. The distribution of dissolved iron in the West Atlantic Ocean. PLoS One 9, e101323. http://dx.doi.org/10.1371/journal.pone.0101323.

Rouxel, O.J., Auro, M., 2010. Iron isotope variations in coastal seawater determined by multicollector ICP-MS. Geostand. Geoanal. Res. 34, 135–144. http://dx.doi.org/10.1111/j.1751-908X.2010.00063.x.

Saito, M.A., Noble, A.E., Tagliabue, A., Goepfert, T.J., Lamborg, C.H., Jenkins, W.J., 2013. Slow-spreading submarine ridges in the South Atlantic as a significant oceanic iron source. Nat. Geosci. 6, 775–779. http://dx.doi.org/10.1038/ngeo1893.

Schlitzer, R., 2015. eGEOTRACES - Electronic Atlas of GEOTRACES Sections and Animated 3D Scenes. http://www.egeotraces.org.

Sedwick, P.N., Church, T.M., Bowie, A.R., Marsay, C.M., Ussher, S.J., Achilles, K.M., Lethaby, P.J., Johnson, R.J., Sarin, M.M., McGillicuddy, D.J., 2005. Iron in the Sargasso Sea (Bermuda Atlantic time-series study region) during summer: Eolian imprint, spatio-temporal variability, and ecological implications. Glob. Biogeochem. Cycles 19, GB4006. http://dx.doi.org/10.1029/2004GB002445.

Sedwick, P.N., Sholkovitz, R., Church, T.M., 2007. Impact of anthropogenic combustion emissions on the fractional solubility of aerosol iron: evidence from the Sargasso Sea. Geochem. Geophys. Geosyst. 8, 1525–2027. http://dx.doi.org/10.1029/2007GC001586.

Siebert, C., Nagler, T.F., Kramers, J.D., 2001. Determination of molybdenum isotope fractionation by double-spike multicollector inductively coupled plasma mass spectrometry. Geochem. Geophys. Geosyst. 2 http://dx.doi.org/10.1029/2000GC000124.

Staubwasser, M., Schoenberg, R., von Blanckenburg, F., Krüger, S., Pohl, C., 2013. Isotope fractionation between dissolved and suspended particulate Fe in the oxic and anoxic water column of the Baltic Sea. Biogeosciences 10, 233–245. http://dx.doi.org/10.5194/bg-10-233-2013.

Steele, R.C.J., Elliott, T., Coath, C.D., Regelous, M., 2011. Confirmation of mass-independent Ni isotopic variability in iron meteorites. Geochim. Cosmochim. Acta 75 (24), 7906–7925. http://dx.doi.org/10.1016/j.gca.2011.08.030.

Villar, E., Farrant, G.K., Follows, M., Garczarek, L., Speich, S., Audic, S., Bittner, L., Blanke, B., Brum, J.R., Brunet, C., Casotti, R., Chase, A., Dolan, J.R., d'Ortenzio, F., Gattuso, J.-P., Grima, N., Guidi, L., Hill, C.N., Jahn, O., Jamet, J.-L., Le Goff, H., Lepoivre, C., Malviya, S., Pelletier, E., Romagnan, J.-B., Roux, S., Santini, S., Scalco, E., Schwenck, S.M., Tanaka, A., Testor, P., Vannier, T., Vincent, F., Zingone, A., Dimier, C., Picheral, M., Searson, S., Kandels-Lewis, S., Acinas, S.G., Bork, P., Boss, E., de Vargas, C., Gorsky, G., Ogata, H., Pesant, S., Sullivan, M.B., Sunagawa, S., Wincker, P., Karsenti, E., Bowler, C., Not, F., Hingamp, P., Iudicone, D., 2015. Ocean plankton. Environmental characteristics of Agulhas rings affect interocean plankton transport. Science 348, 1261447. http://dx.doi.org/10.1126/science.1261447.

Wu, J.F., Boyle, E.A., 2002. Iron in the Sargasso Sea: implications for the processes controlling dissolved Fe distribution in the ocean. Glob. Biogeochem. Cycles 16 (4), 1086. http://dx.doi.org/10.1029/2001GB001453.

Wyatt, N.J., Milne, A., Woodward, E.M.S., Rees, A.P., Browning, T.J., Bouman, H.A., Worsfeld, P.J., Lohan, M.C., 2014. Biogeochemical cycling of dissolved zinc along the GEOTRACES South Atlantic transect GA10 at 40°S. Glob. Biogeochem. Cycles 28, 44–56. http://dx.doi.org/10.1002/2013GB004637.

Zhao, Y., Vance, D., Abouchami, W., de Baar, H.J.W., 2014. Biogeochemical cycling of zinc and its isotopes in the Southern Ocean. Geochim. Cosmochim. Acta 125, 653–672. http://dx.doi.org/10.1016/j.gca.2013.07.045.